Dalton Transactions

ROYAL SOCIETY OF CHEMISTRY

PAPER

View Article Online
View Journal

Cite this: DOI: 10.1039/d5dt03015c

Hydroxyquinoline-functionalised aza-crown macrocycles for lanthanide coordination

Christina Siakalli, [a,b] Bradley E. Osborne, [a,b] Ryan K. Brown,[a] Claudia Rocco,[c] Dominik Weiss,[c] Enrique V. García-España, [d] Pascal V. Grundler,[e] Anzhelika N. Moiseeva,[e] Zeynep Talip,[f] Nicholas P. van der Meulen,[e,f] Michelle T. Ma *[b] and Nicholas J. Long *[a]

Emerging therapeutic radiolanthanides have utility for systemic molecular radiotherapy in nuclear medicine, provided that suitable chemical technology is available to incorporate them into receptor-targeted radiopharmaceuticals. In this work, *N*,*N*′-bis(8-hydroxyquinoline-2-ylmethyl)-4,13-diaza-18-crown-6 (**H_2KHQ**) was synthesised, and its binding ability, thermodynamic stability and selectivity for Ln^{3+} ions (Ln^{3+} = La, Tb, and Lu) investigated. The design of **H_2KHQ** involves pendant arms featuring 8-hydroxyquinoline units, known to possess metal-chelating properties and desirable activity in other therapeutic molecules. **H_2KHQ** exhibited selectivity for the larger Ln^{3+} ions, confirmed by experimentally measured stability constants as well as DFT calculations. **H_2KHQ** was able to bind the larger, non-radioactive La^{3+} and Tb^{3+} ions within 30 minutes at room temperature, forming a single, 2-fold symmetric species in solution. The structure of **[La-HKHQ]$^{2+}$**, as determined by single crystal XRD, emphasized the need for high denticity chelators to satisfy the coordination sphere of the Ln^{3+}, showing a 10-coordinate La^{3+} metal centre. **H_2KHQ** was radiolabelled with [^{161}Tb]$TbCl_3$ under mild conditions in 92% radiochemical yield in promising proof-of-concept measurements.

Received 17th December 2025,
Accepted 25th January 2026

DOI: 10.1039/d5dt03015c

rsc.li/dalton

Introduction

Radioactive nuclides of the lanthanides have significant utility in nuclear medicine for both diagnostic imaging and systemic radiotherapy. In particular, radiolanthanides that emit cytotoxic particles including beta (β^-), alpha (α) and Auger Electrons (AE), have demonstrated efficacy in theranostic radiopharmaceuticals.[1–3] Diagnostic and therapeutic ("theranostic") pairs of radiopharmaceuticals typically utilise the same biologically active receptor-targeted vector to deliver either an imaging radionuclide or a cytotoxic therapeutic radionuclide to diseased tissue. This "look and treat" approach uses the radiotracer, in combination with either Positron Emission Tomography (PET) or Single Photon Emission Computed Tomography (SPECT) imaging to provide diagnostic information that guides decisions on suitability of the companion therapeutic radiotracer.[1,4] For example, the PET radionuclide gallium-68 (^{68}Ga, $t_{1/2}$ = 68 min, β^+) is commonly used in tandem with therapeutic lutetium-177 (^{177}Lu, $t_{1/2}$ = 6.64 days, β^-) for the treatment of somatostatin receptor (SSTR)-positive neuroendocrine tumours, using an "octreotate" peptide attached to a macrocyclic chelator.[3,5,6] While the use of the ^{68}Ga/^{177}Lu radionuclide pair is effective, "true theranostic" agents consisting of a pair of imaging and therapeutic radionuclides of the same element could provide significant advantages. In "true theranostic" pairs, the chemically identical imaging radiotracer and radiotherapeutic agent exhibit equivalent biodistributions: the imaging radiotracer can be used to determine accurate dosimetry of the radiotherapeutic agent. Examples include copper-64/copper-67 (^{64}Cu, β^+/^{67}Cu, β^-), terbium-155/terbium-161 (^{155}Tb, γ/^{161}Tb, β^-, AE, γ) and scandium-44/scandium-47 (^{44}Sc, β^+/^{47}Sc, β^-).[3,7–9] Terbium radioisotopes have potential for receptor-targeted theranostic radiopharmaceuticals. There are four clinically relevant radioisotopes: ^{149}Tb ($t_{1/2}$ = 4.12 hours, E_α = 3.97 MeV, I_α = 16.7%) for targeted α therapy, ^{152}Tb ($t_{1/2}$ = 17.5 hours, $E_{\beta+,av}$ = 1.14 MeV, I = 20.3%) for PET and ^{155}Tb ($t_{1/2}$ = 5.3 days, E_γ = 86.6, 105.3 and 180.1 keV) for SPECT. Finally, ^{161}Tb ($t_{1/2}$ = 6.95 days) is a β^--

[a]*Department of Chemistry, Imperial College London, Molecular Sciences Research Hub, White City Campus, London, W12 0BZ, UK. E-mail: n.long@imperial.ac.uk*
[b]*School of Biomedical Engineering and Imaging Sciences, King's College London, St Thomas' Hospital, London, SE1 7EH, UK. E-mail: michelle.ma@kcl.ac.uk*
[c]*Department of Earth Science and Engineering, Imperial College London, South Kensington Campus, London, SW7 2BP, UK*
[d]*ICMol, Departament de Química Inorgànica, Universitat de València, C/Catedrático José Beltrán 2, Paterna 46980, Spain*
[e]*Center for Radiopharmaceutical Sciences, PSI Center for Life Sciences, 5232 Villigen-PSI, Switzerland*
[f]*Laboratory of Radiochemistry, PSI Center for Nuclear Engineering and Science, 5232 Villigen-PSI, Switzerland*

emitter (154 keV) that undergoes low-energy internal conversion (IC), co-emitting high-energy AE (~12.12 e^-, <40 keV per decay) and γ-rays.[3,7,10] In side-by-side preclinical studies, ^{161}Tb has showcased superior *in vitro* and *in vivo* efficacy compared to ^{177}Lu, alongside an ability to deliver higher absorbed doses.[10–14] The co-emission of both long-range β^- and shorter-range AE emissions from ^{161}Tb in comparison to ^{177}Lu (β^- emitter only) is hypothesized to increase its efficacy and radiotherapeutic effect.[7,15,16] Phase I/II clinical trials with ^{161}Tb radiopharmaceuticals are currently evaluating the efficacy of ^{161}Tb-based radiopharmaceuticals.[17]

A suitable chelating agent is required to coordinate radiolanthanides such as ^{161}Tb and subsequently attach them to biologically active motifs that target surface receptors of diseased cells. Over the years, a series of aza-crown macrocyclic chelators have been developed, for coordination of rare-earth metals available for theranostic applications (Fig. 1). The coordination chemistry of macropa, macrodipa and next-generation analogues have been extensively studied with regards to their ability to bind clinically relevant radionuclides, including actinium-225 (^{225}Ac) and lanthanum-135 (^{135}La).[18–27] Macropa displayed preferential binding with radionuclides of larger ionic radius, over smaller radionuclides whereas macrodipa, py-macrodipa and py_2-macrodipa complexes with both large and small radionuclides demonstrated increased thermodynamic and kinetic stability.[21–23] Blei *et al.* have further highlighted the abilities of macropa to bind radiometals with larger ionic radii (lead-212 (^{212}Pb) and lanthanum-133 (^{133}La)) in 100% radiochemical conversion (RCC), comparable to labelling with ^{225}Ac.[27] Macropa was also able to complex the smaller radionuclide, ^{177}Lu, however, the complex's kinetic stability was lower and higher ligand concentrations were required to achieve satisfactory RCC.[27] Still, macropa is one of the two state-of-the-art chelators for ^{225}Ac, alongside 1,4,7,10-tetraazacyclododecane-1,4,7,10-tetraacetic acid (DOTA) and is currently being used in clinical trials.[28,29]

In this work, we explore a diaza-18-crown-6 derivative, **H_2KHQ**, containing two 8-hydroxyquinoline pendant arms. This chelator is related to macropa, in that the picolinic acid groups of the latter are replaced by 8-hydroxyquinoline motifs. **H_2KHQ** has highly similar topology to macropa, with increased rigidity in the pendant arms. **H_2KHQ** has been previously studied for the complexation of divalent metals ions of zinc, barium, copper, as well as monovalent potassium and sodium.[30] *However, it has not been reported for the complexation of trivalent lanthanides or for use in nuclear medicine*. In general, 8-hydroxyquinoline units and derivatives are widely used in medicinal chemistry and drug discovery.[31–36] They are well-known to possess metal chelating properties and have been assessed as ionophores,[37,38] antiseptic,[39] antioxidant,[40,41] and anticancer agents.[42,43] In addition, they exhibit photophysical properties enabling them to act as sensitizers for Ln^{3+} in a wide variety of applications including biological imaging and materials chemistry.[44–49]

Results

Ligand synthesis

H_2KHQ (*N*,*N*′-bis(8-hydroxyquinoline-2-ylmethyl)-4,13-diaza-18-crown-6) was synthesised in a three-step reaction as shown in Scheme 1. 8-Hydroxyquinoline-2-carbaldehyde was reduced and brominated following a previous procedure.[50] Subsequent attachment of intermediate **2** onto a Kryptofix®22 backbone was carried out *via* nucleophilic substitution in the presence of sodium carbonate, adapted from previous procedures.[24,26] The product was isolated as a pure, white solid in 27% yield post purification (Fig. S1–S6, SI).

Characterisation of lanthanide complexes

To investigate the metal chelating abilities of **H_2KHQ**, the non-radioactive **[Tb-KHQ]$^+$** complex was synthesised by mixing **H_2KHQ** and $TbCl_3{\cdot}6H_2O$ (1.2 eq.) in H_2O (pH 4–5) at room temperature for 30 min. The pure complex was isolated by C18 reverse-phase chromatography as a yellow solid in 65% yield. The ^{1}H NMR spectrum shows no evidence of unchelated **H_2KHQ** ligand and contains characteristic paramagnetic NMR shifts of Tb^{3+}, with signals observed between −200 and +250 ppm (Fig. 2A).[51] LC-MS (Fig. S26) and HR-ESI-MS (Fig. S27) detected a molecular ion peak corresponding to the stoichiometry of **[Tb-KHQ]$^+$** at *m*/*z* 733.2076 (for $[C_{32}H_{38}N_4TbO_6]^+$ calcd = 733.2039). HPLC confirmed the presence of a single **[Tb-KHQ]$^+$** species in solution, with a retention time distinct to that of unchelated **H_2KHQ** ligand (Fig. 2B).

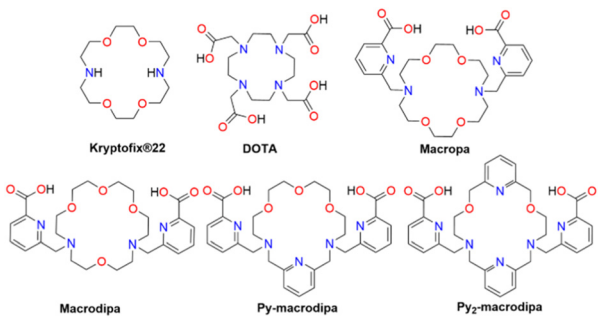

Fig. 1 Examples of azamacrocyclic chelators.

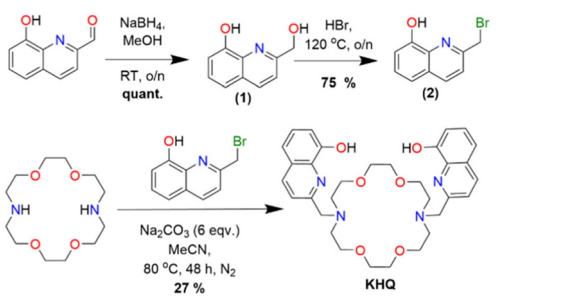

Scheme 1 Synthesis of **H_2KHQ**.

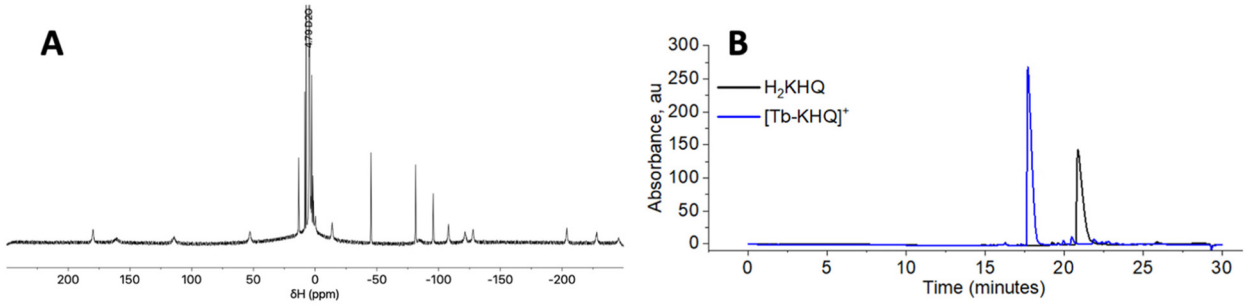

Fig. 2 (A) ^{1}H NMR spectrum of **[Tb-KHQ]$^{+}$** (D_2O, 400 MHz, 298 K). (B) HPLC chromatogram of **H_2KHQ** and **[Tb-KHQ]$^{+}$** (1 mM in NH_4OAc, pH 6.5).

The diamagnetic **[La-KHQ]$^{+}$** complex was also prepared: **H_2KHQ** and $LaCl_3{\cdot}7H_2O$ (1.2 eq.) were mixed in D_2O (pD 6.5) at room temperature for 30 min. The ^{1}H NMR spectrum (Fig. 3) indicated a single symmetric species present: only five resonances in the aromatic region were observed, corresponding to the five distinct proton environments on the 8-hydroxyquinoline arms. Notably, large geminal ^{1}H–^{1}H coupling constants ($^{2}J_{HH}$ > 10 Hz) were observed for all macrocyclic CH_2 protons. This is consistent with metal binding, leading to chemically inequivalent geminal proton environments. In the $^{13}C\{^{1}H\}$ NMR spectrum (Fig. S12), sixteen ^{13}C signals were detected, further supporting the presence of a 2-fold symmetric species. Upon La^{3+} binding, an increase in the chemical shift of aromatic 8-hydroxyquinoline ^{13}C resonances was observed, relative to the unchelated **H_2KHQ** ligand. The chemical equivalence of ^{1}H and ^{13}C atoms of both 8-hydroxyquinoline motifs is similar to analagous complexes (La^{3+}-macrodipa, La^{3+}-macropa), in which 2-fold symmetry was also observed in solution by ^{1}H and ^{13}C NMR spectroscopy.[20,21,52]

To further probe the solution-state chemistry of **[La-KHQ]$^{+}$**, a mixture of **H_2KHQ** and $LaCl_3{\cdot}7H_2O$ (1.2 eq.) in D_2O was monitored *via* ^{1}H NMR spectroscopy from pD 2–13 (Fig. S15). The ^{1}H NMR spectrum of **H_2KHQ** ligand did not change significantly with pD. Binding of La^{3+} to **H_2KHQ** was not observed at low pD but was seen at pD 6.5, with only a single species noted. With increasing pD, the chemical shifts of **[La-KHQ]$^{+}$** did not change significantly.

Lastly, the formation of **[Lu-KHQ]$^{+}$** complex was also explored *via* ^{1}H NMR studies (Fig. S18–S20). **H_2KHQ** and $LuCl_3{\cdot}6H_2O$ (1.2 eq.) were reacted in D_2O, and ^{1}H NMR spectra were obtained over pD 2–9. At low pD, no complex formation was detected whereas at pD 6, **H_2KHQ** ligand and a **[Lu-KHQ]$^{+}$** species were observed in a 1 : 2 ratio. At pD 9, full conversion to a **[Lu-KHQ]$^{+}$** metal complex was observed. Similarly to **[La-KHQ]$^{+}$**, the Lu^{3+} complex showed 2-fold symmetry, as evidenced by a single set of aromatic protons.

To explore the solid-state structure of the **[La-KHQ]$^{+}$** complex, it was re-synthesised by mixing **H_2KHQ** with La$(ClO_4)_3$ (1.2 eq.) in MeOH at room temperature for 30 min. Single crystals of **[La-HKHQ]$(ClO_4)_2$** were obtained by vapour diffusion of pentane into a solution of **[La-HKHQ]$(ClO_4)_2$** in EtOH. Single crystal X-ray diffraction analysis revealed the crystalline material to be **[La-HKHQ]$(ClO_4)_2$** (Fig. 4). The La^{3+} metal centre sits in a 10-coordinate environment, with all nitrogen and oxygen donor atoms bound to the metal centre. The complex adopted a *syn*-conformation, where the 8-hydroxyquinoline arms were both coordinated to the metal centre on the same face relative to the macrocyclic ring. The *syn*-conformation of the ligand implies the presence of two helices, one for the pendant arms (absolute configuration Δ or Λ) and one for the six five-membered chelate rings formed (absolute configuration δ or λ).[53,54] The crystal structure reveals the most

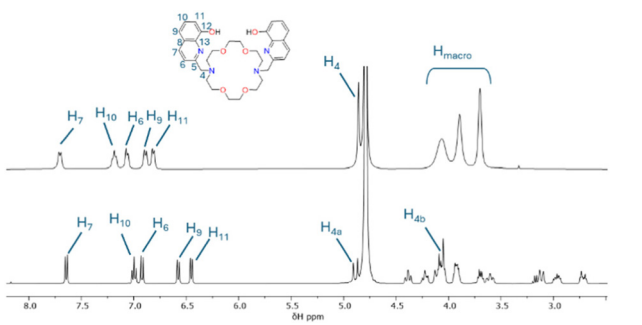

Fig. 3 Expanded ^{1}H NMR spectrum of **H_2KHQ** (top) and **[La-KHQ]$^{+}$** (bottom). (D_2O, pD 6.5, 400 MHz, 298 K). The macrocyclic protons are labelled as H_{macro}.

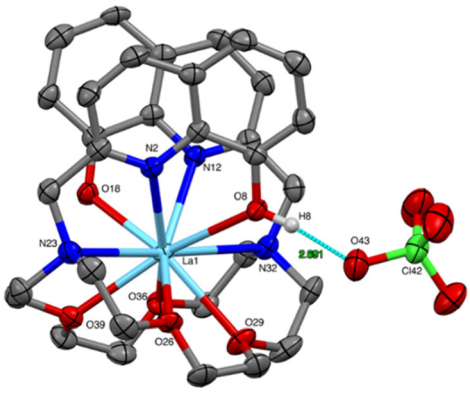

Fig. 4 The structure of **[La-HKHQ]$(ClO_4)_2$** (50% probability ellipsoids). H atoms and second perchlorate anion omitted for clarity. H-bonding contacts in teal and interatomic distances in green.

stable isomer to be Δ(δλλ)(δλδ), present as part of a racemate. One of the hydroxyl groups remained protonated, forming a hydrogen bond to a second perchlorate counter-anion, and a long La–O8 bond (2.673(3) Å). The non-protonated oxygen atom in the 8-hydroxyquinoline arms formed a strong La–O18 bond (2.365(3) Å). In **[La-HKHQ]$^{2+}$**, La–N12 (2.658(4) Å), La–N2 (2.655(3) Å), La–N23 (2.847(4) Å) were all relatively shorter than the La–N bonds in [La(Hmacropa)(H_2O)], suggesting that the 8-hydroxyquinoline arms provide a basis for stronger binding in comparison to the picolinate motif.[20] The solid-state structure was consistent with the ^{1}H NMR solution-state data.

Lanthanide complexes thermodynamic stability

Potentiometric titrations were employed to obtain ligand protonation constants (K_a) and complex stability constants (K_{LnL}) (defined in eqn (S4) and (S5) respectively).

As shown in Table 1, the first and second **H_2KHQ** protonation constants (log K_{H1} and log K_{H2}) correspond to the hydroxyl groups of the two 8-hydroxyquinoline arms. In free 8-hydroxyquinoline, the hydroxyl groups have a pK_a of 9.9.[55] The differences in protonation constants between the two 8-hydroxyquinoline substituents on **H_2KHQ** is likely a result of complex intramolecular hydrogen bonding patterns in the unchelated ligand, such as those between the O–H and the macrocyclic nitrogen atoms (Fig. S9).[56] The third and fourth protonation constants (log K_{H3} and log K_{H4}) correspond to the macrocyclic tertiary amine atoms, while the fifth and sixth protonation constants (log K_{H5} and log K_{H6}) correspond to the nitrogen atoms of the 8-hydroxyquinoline motifs.

The log K_{LnL} values for **H_2KHQ** and similar macrocyclic chelators such as macropa and py$_2$-macrodipa were plotted against the ionic radii of key Ln^{3+} ions (Fig. 5).[21–23,57,58] The affinity of **H_2KHQ** for trivalent cationic lanthanide metal ions decreases as the ionic radius decreases. Importantly, the log K_{LnL} (L = **KHQ^{2-}**, Ln = Tb^{3+}, Lu^{3+}) values were comparable

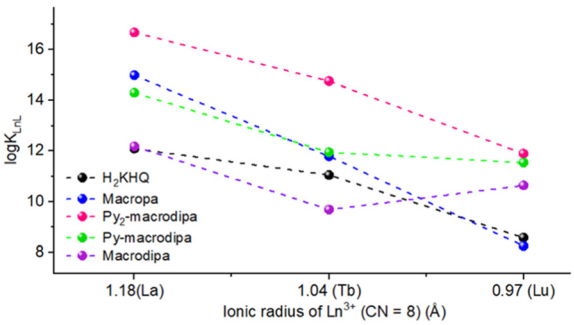

Fig. 5 Stability constants of **[Ln-KHQ]$^+$** (Ln = La, Tb, Lu) plotted *versus* Ln^{3+} ionic radii.

to those of macropa, highlighting that substituting picolinic acid groups for hydroxyquinoline groups does not have a marked effect on the binding affinity of this class of chelators. Indeed, the log K_{LnL} values for Ln^{3+} complexes of **H_2KHQ** are lower than those of many newer chelators (such as py$_2$-macrodipa).

However, to compare ligands with different basicities, the relevant parameter pM, is used as an indicator of affinity (Table 1). The pM value is the negative logarithm of the free metal concentration in equilibrium with complexed and free ligand, at a fixed pH 7.4. Analysis of the pM(Ln(III)) values emphasizes that with **H_2KHQ** at pH 7.4, more Ln(III) ions are present in solution, in comparison to other chelators.

Speciation plots (Fig. 6) indicate that under the conditions studied here, all available **H_2KHQ** ligand molecules were bound to La^{3+} at pH ~6, Tb^{3+} at pH ~6.5 and Lu^{3+} at pH ~7.5. This was also consistent with ^{1}H NMR studies which indicated that a higher pH was needed to achieve quantitative coordination of Lu^{3+} by **H_2KHQ**, as compared to the analogous La^{3+} complex. The distribution of both La^{3+} and Tb^{3+} species supports the formation of one major species at ambient pH, con-

Table 1 Protonation constants (log K_a) and stability constants (log K_{LnL}) obtained by potentiometric titrations

	H_2KHQ[a]	Macropa[24,57]	Py$_2$-macrodipa[23]	Py-macrodipa[22]	Macrodipa[21]
Log K_{a1}	10.40(2)	7.41	7.58(4)	7.20	7.79
Log K_{a2}	7.70(2)	6.85	6.48(1)	6.54	7.04
Log K_{a3}	4.03(4)	3.32	3.52(3)	3.17	3.18
Log K_{a4}	3.74(3)	2.36	2.60(5)	2.31	2.14
Log K_{a5}	3.10(5)	1.69	2.10(11)	—	—
Log K_{a6}	3.08(4)	—	—	—	—
Log K_{LaL}	12.10(8)	14.99	16.68(8)	14.31(6)	12.19(2)
Log K_{TbL}	11.05(2)	11.79	14.76(6)	11.95(3)	9.68(1)
Log K_{LuL}	8.58(5)	8.25	11.90(3)	11.54(2)	10.64(4)
Log K_{LaHL}	—	2.28	—	—	—
Log K_{LuLH-1}	2.46(1)	—	—	—	—
p_{La}	9.47	15.58	17.20	15.03	12.49
p_{Tb}	8.54	12.38	15.28	12.62	9.98
p_{Lu}	7.50	8.84	12.42	12.26	10.94

[a] This work: 0.1 M NaCl, 25 °C. Ligand concentration 0.018 mmol. pH range used 3–10.5. Three repeats. The values in the parentheses are one standard deviation of the last significant figure. pM is the negative logarithm of the free metal concentration in equilibrium with complexed and free ligand, at a fixed pH 7.4.

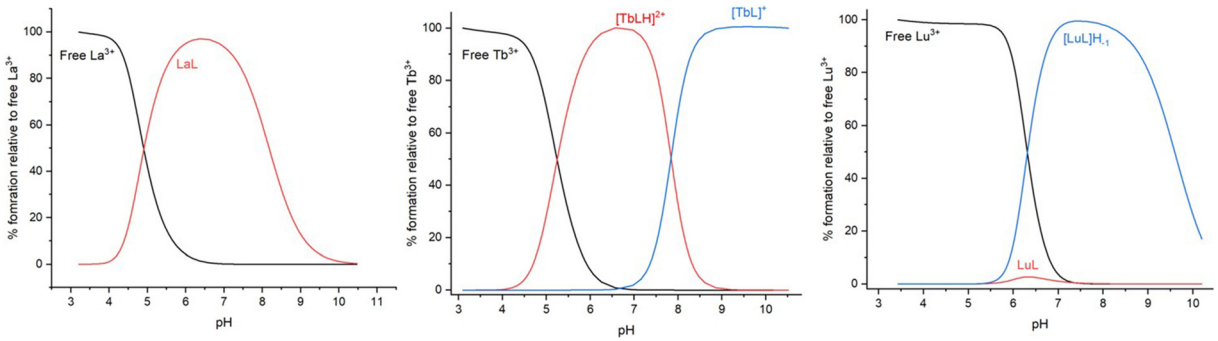

Fig. 6 Representative species distribution for **[Ln-KHQ]**$^{+}$ (Ln = La, Tb, Lu) modelled in HySS. **H_2KHQ** c = 0.018 mmol, Ln^{3+} c = 0.018 mmol. Initial volume V = 30 mL. Data fitting and speciation distribution over the pH range shown. L represents fully deprotonated ligand, KHQ^{2-}.

sistent with ^{1}H NMR spectroscopic studies. Significantly, the Lu^{3+} speciation plot indicates that the major species forming between Lu^{3+} and **H_2KHQ** at above pH 6.5 is LuL_{H-1}. This most likely corresponds to a species where a water molecule is interacting with the complex. Attempts to elucidate the solid-state structure of **[Lu-KHQ]**$^{+}$ *via* crystals were unsuccessful.

DFT calculations

DFT is a useful tool for exploring the coordination chemistry of Ln^{3+} with macrocyclic chelators and has been used to better understand the origin of size selectivity in macropa and second-generation analogues.[21–23] Herein, we explored the binding of **H_2KHQ** across the lanthanide series (La^{3+}–Lu^{3+}) to gain insight into the size selectivity of **H_2KHQ** complexation. Initially, geometries were taken from the crystal structure of *syn* **[La-HKHQ]**$^{2+}$ with removal of H8 to model the overall '+1' species. Different conformational arrangements were modelled with the 8-hydroxyquinoline arms in either a *syn* or *anti* arrangement around the metal centre (whilst retaining symmetry). Across the lanthanide series, the *syn* conformation was favoured over the *anti*-conformation (Fig. S30). The relative Gibbs free energy ($\Delta\Delta G$) for the transmetallation reaction ($[LaKHQ]^{+}$ + Ln^{3+} → $[LnKHQ]^{+}$ + La^{3+}) was calculated. The results show a thermodynamic preference for the larger Ln^{3+} ions (Fig. 7). This calculated trend is in good qualitative agreement with experimental data ($\Delta\Delta G_{exp} = -2.303RT\log(K_{LnL} - K_{LaL})$, $\Delta\Delta G_{Tb-La}$ = +1.43 kcal mol^{-1}, $\Delta\Delta G_{Tb-La}$ = +4.80 kcal mol^{-1}) which shows decreasing thermodynamic stability across the series. The quantitative discrepancy is attributed to the over estimation of gas-phase Ln^{3+} ion energies in our model, which does not include explicit solvation effects. The destabilisation evidently results from a greater degree of ligand strain in the macrocyclic framework to facilitate the coordination of the oxygen atoms to the smaller Ln^{3+} ions (Fig. S34). Furthermore, **H_2KHQ** did not exhibit the conformational toggle that is predominant in macrodipa and analogues.[21–23]

Structural analysis revealed a coordination number of 10 for all Ln^{3+}, involving four nitrogen atoms and six oxygen atoms in coordination to the metal centre (Fig. S31). Across

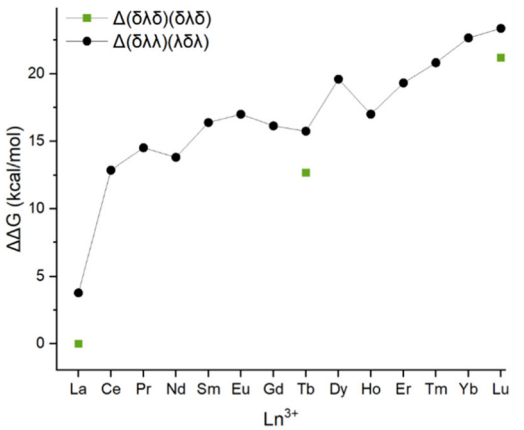

Fig. 7 DFT-computed relative Gibbs free energies ($\Delta\Delta G$) for the transmetallation reaction: values are calculated as: $\Delta G^{\circ}_{hyd}\Delta\Delta G^{\circ} = G^{\circ}_{aq}([syn\text{-Ln-KHQ}]^{+}) + G^{\circ}_{aq}(La^{3+}) - G^{\circ}_{aq}(Ln^{3+}) - G^{\circ}_{aq}([syn\text{-La-KHQ}]^{+})$.

the series, the hapticity of the **KHQ** ligand was η^{10}, with the metal ion located above the plane of the macrocyclic ring system, enclosed by both 8-hydroxyquinoline units. Additionally, the presence of a water molecule in the first coordination sphere was modelled, however the resulting coordination number of 11 was less favoured across the series (Table S2, ΔG°_{hyd}).

Analysis of the structure of $[La\text{-HKHQ}]^{2+}$ reveals that there are 16 possible conformations (8 enantiomeric pairs of diastereoisomers) with C_2 symmetry.[24] To better explore the in-solution behaviour, an in-depth conformational screen of 8 different diastereomers was carried out for La^{3+}, Tb^{3+} and Lu^{3+}. As shown in Fig. S32, our calculations predict that the Δ(δλδ)(δλδ) conformation is the lowest energy form in aqueous solution across the three Ln^{3+} ions tested, and is lower in energy by *ca.* 1.9 kcal mol^{-1} than the solid-state conformation observed for $[La\text{-HKHQ}]^{2+}$. The relative energies of the different conformations in aqueous solution are given in Table S3 and highlight the multiple C_2-symmetric conformational modes that likely exist in equilibrium in solution. This result is consistent with the NMR solution-state studies

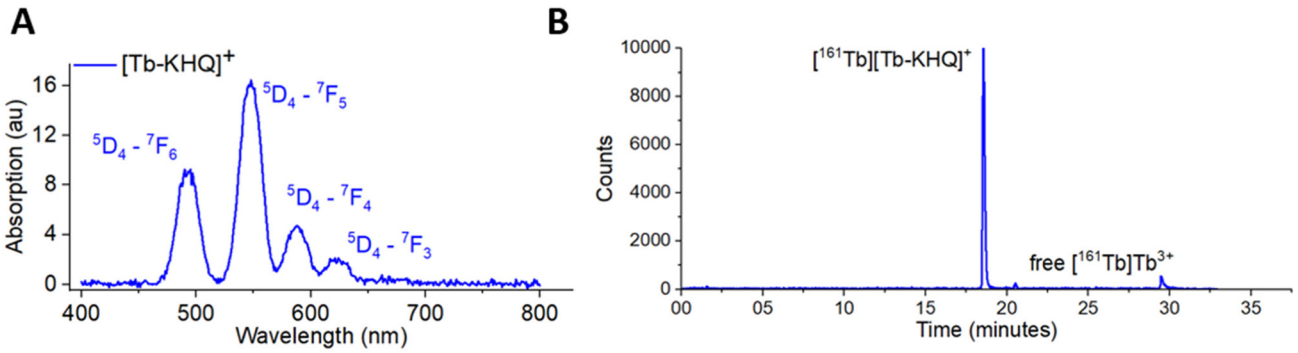

Fig. 8 (A) Phosphorescence spectrum for **[Tb-KHQ]**$^+$ (H_2O, 20 μM, 20 nm slits, 0.1 ms delay). (B) RadioHPLC of **H_2KHQ** (1 mM) with [^{161}Tb]Tb^{3+} (2.5 MBq, 1 mM HCl) after 60 min at 90 °C. RCY = 92%. **[^{161}Tb][Tb-KHQ]**$^+$ retention time = 18.3 min.

on [La-KHQ]$^+$ where a complex with C_2 symmetry was observed.

To explore the effects of the nature of the pendant arm on the stability of these complexes a parallel conformational screen of macropa complexes (for La^{3+}, Tb^{3+} and Lu^{3+}) was carried out, where our model also favoured the Δ(δλδ)(δλδ) conformation (see Fig. S33). Analysis of gas-phase Gibbs free binding energies and ligand strain was performed to compare the influence of the pendant arms of macropa and KHQ on ligand preorganisation and metal binding. The results show that whilst ligand strain generally increases with decreasing ionic radius for both ligands, the effect is much less pronounced for macropa (Fig. S34). Additionally, our calculations suggest that macropa provides a consistently greater, albeit modest, metal–ligand stabilisation for La^{3+}, Tb^{3+} and Lu^{3+} (Table S4). Whilst experiments show the reverse trend for Lu^{3+}, the differences are small enough that calculated values are likely within error. Together with experimental results, it appears that the greater rigidity of the pendant arms in KHQ forces a higher degree of overall ligand strain in the metal-bound conformation of the macrocycle.

Phosphorescence spectroscopy

The pendant 8-hydroxyquinoline motifs possess useful photophysical properties and can potentially act as antennae to exploit the luminescence emission properties of Tb^{3+}. Luminescence studies were carried out to ascertain whether the [Tb-KHQ]$^+$ complex exhibited characteristic Tb phosphorescent emissions. Indeed, sharp emission peaks at 518, 565, 583 and 621 nm were observed for [Tb-KHQ]$^+$ *via* the antenna effect, following excitation of the ligand at 242 nm (Fig. 8A). These are characteristic of the $^5D_4 \rightarrow {}^7F_n$ transitions (n = 6, 5, 4, 3). This preliminary experiment highlights the potential of 8-hydroxyquinoline based ligands to be used for optical imaging, with further studies needed to optimise ligand design for efficient sensitization.

Radiolabelling experiments

Finally, [^{161}Tb]Tb^{3+} radiolabelling experiments were undertaken, with [^{161}Tb]TbCl$_3$ provided by the Paul Scherrer Institute. Solutions of **H_2KHQ** (1 mM) and [^{161}Tb]Tb^{3+} (2.5 MBq, 1 mM HCl) in NH_4OAc (20 mM) at pH 8.5 were reacted at 25 °C. After 20 min and 180 min, the reactions were analysed by reverse-phase radio-HPLC (Fig. S41–43), which indicated formation of **[^{161}Tb][Tb-KHQ]**$^+$ with a retention time (R_t) of 18.33 min. We observed that unreacted [^{161}Tb]Tb^{3+} was initially retained on the column, presumably as a colloidal species, similar to prior radiochemical observations.[59] However, upon switching to an aqueous mobile phase at the end of analysis, free [^{161}Tb]Tb^{3+} eluted, appearing at >29 min, enabling quantification of radiochemical yield (RCY). Preliminary radiolabelling studies show that at 25 °C, **H_2KHQ** was radiolabelled in 33% RCY after 20 min, which increased to 68% after 180 min. Upon heating to 90 °C for 60 min, a high RCY of 92% was achieved (Fig. 8B). In comparison, macropa radiolabelling with [^{161}Tb]Tb^{3+} (5 MBq, 2 mM HCl) was achieved at 62 and 55% RCY respectively at room temperature and 90 °C after 30 minutes (Fig. S44 and S45).

Conclusions

The coordination of **H_2KHQ** with Ln^{3+} ions has been interrogated *via* X-ray crystallography, NMR spectroscopy, DFT calculations, analytical chromatography and potentiometric titrations. **H_2KHQ** exhibited a higher binding affinity towards larger Ln^{3+} ions compared to the smaller ions. DFT calculations corroborate the experimental evidence: **[Ln-KHQ]**$^+$ complexes demonstrated decreasing thermodynamic stability as ionic radii decrease across the lanthanide series. In solid-state studies, XRD analysis of **[La-KHQ]**$^+$ showed that the La^{3+} metal ion adopts a 10-coordinate conformation with the 8-hydroxyquinoline arms binding in a *syn* orientation relative to the macrocycle. This was consistent with solution-state NMR studies, that suggest a 2-fold symmetric complex present. The optical properties of **[Tb-KHQ]**$^+$ were investigated by ligand sensitization at 242 nm, and characteristic phosphorescence emission peaks were observed. It has been noted that in order to effectively exploit the capabilities of 8-HQ moieties as antennae, optimised ligand analogues can be designed for increased

sensitization and signal enhancement. The promising chelation properties seen with La^{3+} and Tb^{3+} prompted us to explore the chelation of **KHQ** with $[^{161}Tb]Tb^{3+}$. Preliminary radiolabelling corroborated the ability of **H_2KHQ** to coordinate $[^{161}Tb]Tb^{3+}$ in high radiochemical yields (92%). Further in-depth radiolabelling studies are required to explore concentration, time, pH and temperature dependencies as well as maximum molar activity. Complex stability and inertness for *in vivo* applications shall be adequately explored in future work. Still, the combination of radioactive properties with photophysical properties could enable the development of a dual-modal Tb^{3+} probe for future medical applications.[60,61]

Author contributions

C. S. synthesised the compounds and performed the analyses. The radiolabelling was performed with the help of B. E.O. and M. T. M. DFT and X-ray crystallography was carried out by R. K. B. Potentiometric titrations were performed by C. S. and C. R. M. T. M. and N. J. L. supervised the project, and all the authors contributed to the writing of the manuscript.

Conflicts of interest

There are no conflicts to declare.

Data availability

The data supporting this article have been included as part of the supplementary information (SI). Supplementary information is available. See DOI: https://doi.org/10.1039/d5dt03015c.

CCDC 2435038 and 2435039 contain the supplementary crystallographic data for this paper.[62a,b]

Acknowledgements

The research was supported by the EPSRC programme for Next Generation Molecular Imaging and Therapy with Radionuclides (EP/S019901/1, "MITHRAS"), the EPSRC Centre for Doctoral Training in Smart Medical Imaging (EP/S022104/1), and as part of the PRISMAP project supported by the European Union's Horizon 2020 research and innovation program under grant agreement no. 101008571. CR acknowledges funding from the Marie Sklodowska-Curie grant agreement no. [101032337].

References

1 T. I. Kostelnik and C. Orvig, Radioactive Main Group and Rare Earth Metals for Imaging and Therapy, *Chem. Rev.*, 2019, **119**, 902–956.
2 A. Hu and J. J. Wilson, in *Radiopharmaceutical Therapy*, Springer International Publishing, 2023, pp. 123–144.
3 N. Naskar and S. Lahiri, Theranostic Terbium Radioisotopes: Challenges in Production for Clinical Application, *Front. Med.*, 2021, **8**, 675014.
4 F. Rösch and R. P. Baum, Generator-based PET radiopharmaceuticals for molecular imaging of tumours: on the way to THERANOSTICS, *Dalton Trans.*, 2011, **40**, 6104.
5 H. Duan and A. Iagaru, in *Radiopharmaceutical Therapy*, Springer International Publishing, Cham, 2023, pp. 455–481.
6 J. R. Ballinger, Theranostic radiopharmaceuticals: established agents in current use, *Br. J. Radiol.*, 2018, **91**, 20170969.
7 C. Van Laere, M. Koole, C. M. Deroose, M. Van de Voorde, K. Baete, T. E. Cocolios, C. Duchemin, M. Ooms and F. Cleeren, Terbium radionuclides for theranostic applications in nuclear medicine: from atom to bedside, *Theranostics*, 2024, **14**, 1720–1743.
8 B. A. Vaughn, A. J. Koller, Z. Chen, S. H. Ahn, C. S. Loveless, S. J. Cingoranelli, Y. Yang, A. Cirri, C. J. Johnson, S. E. Lapi, K. W. Chapman and E. Boros, Homologous Structural, Chemical, and Biological Behavior of Sc and Lu Complexes of the Picaga Bifunctional Chelator: Toward Development of Matched Theranostic Pairs for Radiopharmaceutical Applications, *Bioconjugate Chem.*, 2021, **32**, 1232–1241.
9 B. A. Vaughn, C. S. Loveless, S. J. Cingoranelli, D. Schlyer, S. E. Lapi and E. Boros, Evaluation of 177Lu and 47Sc Picaga-Linked, Prostate-Specific Membrane Antigen-Targeting Constructs for Their Radiotherapeutic Efficacy and Dosimetry, *Mol. Pharm.*, 2021, **18**, 4511–4519.
10 C. Müller, J. Reber, S. Haller, H. Dorrer, P. Bernhardt, K. Zhernosekov, A. Türler and R. Schibli, Direct in vitro and in vivo comparison of 161Tb and 177Lu using a tumour-targeting folate conjugate, *Eur. J. Nucl. Med. Mol. Imaging*, 2014, **41**, 476–485.
11 J. Grünberg, D. Lindenblatt, H. Dorrer, S. Cohrs, K. Zhernosekov, U. Köster, A. Türler, E. Fischer and R. Schibli, Anti-L1CAM radioimmunotherapy is more effective with the radiolanthanide terbium-161 compared to lutetium-177 in an ovarian cancer model, *Eur. J. Nucl. Med. Mol. Imaging*, 2014, **41**, 1907–1915.
12 C. Müller, C. A. Umbricht, N. Gracheva, V. J. Tschan, G. Pellegrini, P. Bernhardt, J. R. Zeevaart, U. Köster, R. Schibli and N. P. van der Meulen, Terbium-161 for PSMA-targeted radionuclide therapy of prostate cancer, *Eur. J. Nucl. Med. Mol. Imaging*, 2019, **46**, 1919–1930.
13 P. Bernhardt, J. Svensson, J. Hemmingsson, N. P. van der Meulen, J. R. Zeevaart, M. W. Konijnenberg, C. Müller and J. Kindblom, Dosimetric Analysis of the Short-Ranged Particle Emitter 161Tb for Radionuclide Therapy of Metastatic Prostate Cancer, *Cancers*, 2021, **13**, 2011.
14 E. Hindie, P. Zanotti-Fregonara, M. A. Quinto, C. Morgat and C. Champion, Dose deposits from90Y,177Lu,111In, and161Tb in micrometastases of various sizes: Implications for radiopharmaceutical therapy, *J. Nucl. Med.*, 2016, **57**, 759–764.

15 D. Wild and M. Fani, in *Radiopharmaceutical Therapy*, Springer International Publishing, Cham, 2023, pp. 335–348.
16 K. M. Wulfmeier, J. Cheng, I. M. Costa, A. Rigby, L. Livieratos, R. Fernandez, P. J. Blower, K. A. Vallis, R. M. Reilly, G. Pirovano and S. Y. A. Terry, in *Radiopharmaceutical Therapy*, Springer International Publishing, Cham, 2023, pp. 409–434.
17 J. P. Buteau, L. Kostos, R. Alipour, P. Jackson, L. McInstosh, B. Emmerson, M. B. Haskali, J. Xie, E. Medhurst, R. Ravi, B. D. Gonzalez, H. Fettke, B. Blyth, L. Furic, K. Owen, S. Sandhu, D. G. Murphy, A. A. Azad and M. S. Hofman, Clinical Trial Protocol for VIOLET: A Single-Center, Phase I/II Trial Evaluation of Radioligand Treatment in Patients with Metastatic Castration-Resistant Prostate Cancer with [161Tb]Tb-PSMA-I&T, *J. Nucl. Med.*, 2024, **65**, 1231–1238.
18 R. Ferreirós-Martínez, D. Esteban-Gómez, E. Tóth, A. De Blas, C. Platas-Iglesias and T. Rodríguez-Blas, Macrocyclic receptor showing extremely high Sr(II)/Ca(II) and Pb(II)/Ca(II) selectivities with potential application in chelation treatment of metal intoxication, *Inorg. Chem.*, 2011, **50**, 3772–3784.
19 M. P. Jensen, R. Chiarizia, I. A. Shkrob, J. S. Ulicki, B. D. Spindler, D. J. Murphy, M. Hossain, A. Roca-Sabio, C. Platas-Iglesias, A. De Blas and T. Rodríguez-Blas, Aqueous complexes for efficient size-based separation of americium from curium, *Inorg. Chem.*, 2014, **53**, 6003–6012.
20 N. A. Thiele, V. Brown, J. M. Kelly, A. Amor-Coarasa, U. Jermilova, S. N. MacMillan, A. Nikolopoulou, S. Ponnala, C. F. Ramogida, A. K. H. Robertson, C. Rodríguez-Rodríguez, P. Schaffer, C. Williams, J. W. Babich, V. Radchenko and J. J. Wilson, An Eighteen–Membered Macrocyclic Ligand for Actinium–225 Targeted Alpha Therapy, *Angew. Chem.*, 2017, **129**, 14904–14909.
21 A. Hu, S. N. MacMillan and J. J. Wilson, Macrocyclic Ligands with an Unprecedented Size-Selectivity Pattern for the Lanthanide Ions, *J. Am. Chem. Soc.*, 2020, **142**, 13500–13506.
22 A. Hu, E. Aluicio-Sarduy, V. Brown, S. N. Macmillan, K. V. Becker, T. E. Barnhart, V. Radchenko, C. F. Ramogida, J. W. Engle and J. J. Wilson, Py-Macrodipa: A Janus Chelator Capable of Binding Medicinally Relevant Rare-Earth Radiometals of Disparate Sizes, *J. Am. Chem. Soc.*, 2021, **143**, 10429–10440.
23 A. Hu, M. E. Simms, V. Kertesz, J. J. Wilson and N. A. Thiele, Chelating Rare-Earth Metals (Ln3+) and 225Ac3 + with the Dual-Size-Selective Macrocyclic Ligand Py2-Macrodipa, *Inorg. Chem.*, 2022, **61**, 12847–12855.
24 A. Roca-Sabio, M. Mato-Iglesias, D. Esteban-Gómez, É. Toth, A. De Bias, C. Platas-Iglesias and T. Rodríguez-Blas, Macrocyclic receptor exhibiting unprecedented selectivity for light lanthanides, *J. Am. Chem. Soc.*, 2009, **131**, 3331–3341.
25 A. Hu, K. E. Martin, D. Śmiłowicz, E. Aluicio-Sarduy, S. J. Cingoranelli, S. E. Lapi, J. W. Engle, E. Boros and J. J. Wilson, Construction of the Bioconjugate Py–Macrodipa–PSMA and Its In Vivo Investigations with Large 132/135 La 3 + and Small 47 Sc 3+ Radiometal Ions, *Eur. J. Inorg. Chem.*, 2023, **26**, DOI: 10.1002/ejic.202300457.
26 M. Mato-Iglesias, A. Roca-Sabio, Z. Pálinkás, D. Esteban-Gómez, C. Platas-Iglesias, É. Tóth, A. De Blas and T. Rodríguez-Blas, Lanthanide complexes based on a 1,7-diaza-12-crown-4 platform containing picolinate pendants: A new structural entry for the design of magnetic resonance imaging contrast agents, *Inorg. Chem.*, 2008, **47**, 7840–7851.
27 M. K. Blei, L. Waurick, F. Reissig, K. Kopka, T. Stumpf, B. Drobot, J. Kretzschmar and C. Mamat, Equilibrium Thermodynamics of Macropa Complexes with Selected Metal Isotopes of Radiopharmaceutical Interest, *Inorg. Chem.*, 2023, **62**, 20699–20709.
28 C. A. Schatz, S. Zitzmann-Kolbe, I. Moen, M. Klotz, S. Nair, S. Stargard, R. M. Bjerke, K. Wickstrøm Biseth, Y. Z. Feng, B. Indrevoll, V. Cruciani, J. Karlsson, B. Haendler, C. H. Nielsen, M. Z. Alfsen, S. Hammer, H. Hennekes, A. Cuthbertson, U. B. Hagemann and Å. Larsen, Preclinical Efficacy of a PSMA-Targeted Actinium-225 Conjugate (225Ac-Macropa-Pelgifatamab): A Targeted Alpha Therapy for Prostate Cancer, *Clin. Cancer Res.*, 2024, **30**, 2531–2544.
29 N. A. Thiele and J. J. Wilson, Actinium-225 for Targeted α Therapy: Coordination Chemistry and Current Chelation Approaches, *Cancer Biother. Radiopharm.*, 2018, **33**, 336–348.
30 N. Su, J. S. Bradshaw, X. X. Zhang, H. Song, P. B. Savage, G. Xue, K. E. Krakowiak and R. M. Izatt, Syntheses and metal ion complexation of novel 8-hydroxyquinoline- containing diaza-18-crown-6 ligands and analogues, *J. Org. Chem.*, 1999, **64**, 8855–8861.
31 V. Prachayasittikul, V. Prachayasittikul, S. Prachayasittikul and S. Ruchirawat, 8-Hydroxyquinolines: a review of their metal chelating properties and medicinal applications, *Drug Des., Dev. Ther.*, 2013, **7**, 1157.
32 V. Oliveri and G. Vecchio, 8-Hydroxyquinolines in medicinal chemistry: A structural perspective, *Eur. J. Med. Chem.*, 2016, **120**, 252–274.
33 A. Cipurković, E. Horozić, S. Marić, L. Mekić and H. Junuzović, Metal Complexes with 8-Hydroxyquinoline: Synthesis and *In Vitro* Antimicrobial Activity, *Open J. Appl. Sci.*, 2021, **11**, 1–10.
34 Y. Song, H. Xu, W. Chen, P. Zhan and X. Liu, 8-Hydroxyquinoline: a privileged structure with a broad-ranging pharmacological potential, *MedChemComm*, 2015, **6**, 61–74.
35 G. J. Kharadi, J. R. Patel and B. Z. Dholakiya, Antituberculosis, antifungal and thermal activity of mixed ligand transition metal complexes, *Appl. Organomet. Chem.*, 2010, **24**, 821–827.
36 R. Gupta, V. Luxami and K. Paul, Insights of 8-hydroxyquinolines: A novel target in medicinal chemistry, *Bioorg. Chem.*, 2021, **108**, 104633.
37 P. J. Gawne, F. Clarke, K. Turjeman, A. P. Cope, N. J. Long, Y. Barenholz, S. Y. A. Terry and R. T. M. de Rosales, PET

imaging of liposomal glucocorticoids using 89Zr-oxine: Theranostic applications in inflammatory arthritis, *Theranostics*, 2020, **10**, 3867–3879.

38 P. Gawne, F. Man, J. Fonslet, R. Radia, J. Bordoloi, M. Cleveland, P. Jimenez-Royo, A. Gabizon, P. J. Blower, N. Long and R. T. M. De Rosales, Manganese-52: applications in cell radiolabelling and liposomal nanomedicine PET imaging using oxine (8-hydroxyquinoline) as an ionophore, *Dalton Trans.*, 2018, **47**, 9283–9293.

39 K. H. Neldner, The Halogenated 8–Hydroxyquinolines, *Int. J. Dermatol.*, 1977, **16**, 267–273.

40 M. I. Fernández-Bachiller, C. Pérez, G. C. González-Muñoz, S. Conde, M. G. López, M. Villarroya, A. G. García and M. I. Rodríguez-Franco, Novel Tacrine−8-Hydroxyquinoline Hybrids as Multifunctional Agents for the Treatment of Alzheimer's Disease, with Neuroprotective, Cholinergic, Antioxidant, and Copper-Complexing Properties, *J. Med. Chem.*, 2010, **53**, 4927–4937.

41 D. Mechlovich, T. Amit, S. A. Mandel, O. Bar-Am, K. Bloch, P. Vardi and M. B. H. Youdim, The Novel Multifunctional, Iron-Chelating Drugs M30 and HLA20 Protect Pancreatic β-Cell Lines from Oxidative Stress Damage, *J. Pharmacol. Exp. Ther.*, 2010, **333**, 874–882.

42 C. Bissani Gasparin and D. A. Pilger, 8–Hydroxyquinoline, Derivatives and Metal–Complexes: A Review of Antileukemia Activities, *ChemistrySelect*, 2023, **8**, DOI: 10.1002/slct.202204219.

43 A. Y. Shaw, C.-Y. Chang, M.-Y. Hsu, P.-J. Lu, C.-N. Yang, H.-L. Chen, C.-W. Lo, C.-W. Shiau and M.-K. Chern, Synthesis and structure-activity relationship study of 8-hydroxyquinoline-derived Mannich bases as anticancer agents, *Eur. J. Med. Chem.*, 2010, **45**, 2860–2867.

44 H. B. Xu, J. Li, L. X. Shi and Z. N. Chen, Sensitized luminescence in dinuclear lanthanide(iii) complexes of bridging 8-hydroxyquinoline derivatives with different electronic properties, *Dalton Trans.*, 2011, **40**, 5549–5556.

45 A. Nonat, D. Imbert, J. Pécaut, M. Giraud and M. Mazzanti, Structural and Photophysical Studies of Highly Stable Lanthanide Complexes of Tripodal 8-Hydroxyquinolinate Ligands Based on 1,4,7-Triazacyclononane, *Inorg. Chem.*, 2009, **48**, 4207–4218.

46 H. Camargo, T. B. Paolini, E. Niyama, H. F. Brito and M. Cremona, New rare-earth quinolinate complexes for organic light-emitting devices, *Thin Solid Films*, 2013, **528**, 36–41.

47 N. M. Shavaleev, R. Scopelliti, F. Gumy and J. C. G. Bünzli, Near-infrared luminescence of nine-coordinate neodymium complexes with benzimidazole-substituted 8-hydroxyquinolines, *Inorg. Chem.*, 2008, **47**, 9055–9068.

48 F. Rizzo, F. Meinardi, R. Tubino, R. Pagliarin, G. Dellepiane and A. Papagni, Synthesis of 8-hydroxyquinoline functionalised DO3A ligand and Eu(iii) and Er(iii) complexes: Luminescence properties, *Synth. Met.*, 2009, **159**, 356–360.

49 Rohini, K. Paul and V. Luxami, 8-Hydroxyquinoline Fluorophore for Sensing of Metal Ions and Anions, *Chem. Rec.*, 2020, **20**, 1430–1473.

50 M. El Safadi, M. Bhadbhade, R. Shimmon, A. T. Baker and A. M. McDonagh, Cyclen-based chelators for the inhibition of Aβ aggregation: Synthesis, anti-oxidant and aggregation evaluation, *Inorg. Chim. Acta*, 2017, **467**, 343–350.

51 A. Dalal, A. Hooda, K. Nehra, D. Singh, S. Kumar, R. S. Malik and P. Kumar, Effect of substituted 2,2′-bipyridine derivatives on luminescence characteristics of green emissive terbium complexes: Spectroscopic and optical analysis, *J. Mol. Struct.*, 2022, **1265**, 133343.

52 A. Hu and J. J. Wilson, Advancing Chelation Strategies for Large Metal Ions for Nuclear Medicine Applications, *Acc. Chem. Res.*, 2022, **55**, 904–915.

53 E. J. Corey and J. C. Bailar, The Stereochemistry of Complex Inorganic Compounds. XXII. Stereospecific Effects in Complex Ions 1, *J. Am. Chem. Soc.*, 1959, **81**, 2620–2629.

54 J. K. Beattie, Conformational analysis of tris(ethylenediamine) complexes, *Acc. Chem. Res.*, 1971, **4**, 253–259.

55 A. Albert and J. N. Phillips, 264. Ionization constants of heterocyclic substances. Part II. Hydroxy-derivatives of nitrogenous six-membered ring-compounds, *J. Chem. Soc.*, 1956, 1294.

56 F. Cuenot, M. Meyer, E. Espinosa, A. Bucaille, R. Burgat, R. Guilard and C. Marichal-Westrich, New insights into the complexation of lead(ii) by 1,4,7,10- tetrakis(carbamoylmethyl)-1,4,7,10-tetraazacyclododecane (DOTAM): Structural, thermodynamic, and kinetic studies, *Eur. J. Inorg. Chem.*, 2008, 267–283.

57 N. A. Thiele, S. N. Macmillan and J. J. Wilson, Rapid Dissolution of BaSO 4 by Macropa, an 18-Membered Macrocycle with High Affinity for Ba 2+, *J. Am. Chem. Soc.*, 2018, **140**, 17071–17078.

58 *CRC Handbook of Chemistry and Physics*, ed. W. M. Haynes, D. R. Lide and T. J. Bruno, CRC Press, Boca Raton, 97th edn, 2016.

59 A. P. Olson, B. R. Schrage, M. F. Islam, L. S. Fletcher, F. Verich, M. A. Dierolf, E. Aluicio-Sarduy, K. V. Becker, D. M. Driscoll, N. Girish, M. E. Simms, V. Kertesz, F. D. White, E. Boros, A. S. Ivanov, J. W. Engle and N. A. Thiele, Towards the Stable Chelation of Radioantimony(v) for Targeted Auger Theranostics, *Angew. Chem., Int. Ed.*, 2025, **64**, DOI: 10.1002/anie.202423878.

60 G. Nizou, C. Favaretto, F. Borgna, P. V. Grundler, N. Saffon-Merceron, C. Platas-Iglesias, O. Fougère, O. Rousseaux, N. P. van der Meulen, C. Müller, M. Beyler and R. Tripier, Expanding the Scope of Pyclen-Picolinate Lanthanide Chelates to Potential Theranostic Applications, *Inorg. Chem.*, 2020, **59**, 11736–11748.

61 M. A. Joaqui-Joaqui, G. G. Sands, D. Śmiłowicz, M. J. Gork, E. Aluicio-Sarduy, T. E. Barnhart, J. W. Engle and E. Boros, A Trifunctional, Rare-Earth Theranostic Chelator Platform to Enable Diagnostic Nuclear Imaging, Surgical Resection, and Radiotherapy, *J. Am. Chem. Soc.*, 2025, **147**, 45303–45314.

62 (*a*) CCDC 2435038: Experimental Crystal Structure Determination, 2026, DOI: 10.5517/ccdc.csd.cc2mqvmv; (*b*) CCDC 2435039: Experimental Crystal Structure Determination, 2026, DOI: 10.5517/ccdc.csd.cc2mqvnw.